Cold gas microthruster

How Cheah, Kean; Ganani, Chaggai; Lemmer, Kristina; Cervone, Angelo

DOI
10.1016/B978-0-12-819037-1.00006-2

Publication date
2022

Document Version
Final published version

Published in
Space Micropropulsion for Nanosatellites

CHAPTER

Cold gas microthruster

2

Kean How Cheah, PhD [1], Chaggai Ganani, MSc [2], Kristina Lemmer, PhD [3], Angelo Cervone, PhD [4]

[1]*Assistant Professor, School of Aerospace, Faculty of Science and Engineering, University of Nottingham Ningbo China, Ningbo, Zhejiang, China;* [2]*Graduate Student, Aerospace Engineering Faculty, Delft University of Technology, Delft, the Netherlands;* [3]*Associate Professor, Department of Mechanical and Aerospace Engineering, Western Michigan University, Kalamazoo, MI, United States;* [4]*Assistant Professor, Aerospace Engineering Faculty, Delft University of Technology, Delft, the Netherlands*

2.1 Background and principles of operation

The cold gas propulsion system is the simplest form of all space propulsions. Historically, it has been used as a reaction control system for more than 50 years. They are not only used as an in-space propulsion system for spacecraft, satellites, and interplanetary landers but also find applications in the launch vehicle. For instance, the Pegasus launch vehicle uses cold gas thrusters in controlling roll axis motion [1]. The reusable first stage rocket of Falcon 9 launch vehicle from SpaceX uses the cold gas thrusters for stabilization before falling back to Earth.

A typical cold gas propulsion system consists of a high-pressure gas tank, a pressure regulator, one or more nozzles, an electrical valve for each nozzle, and slots for filling and venting of the gas, as schematically illustrated in (Fig. 2.1).

The operational principle of the cold gas propulsion system is rather simple. The gas propellant stored at high pressure is vaporized or sublimated via a phase change process into gas, which is vented through a valve into a converging-diverging (CD) nozzle, accelerating the gas flow into high velocity to produce thrust.

The gas flow through the nozzle is primarily driven by the pressure difference between the settling chamber, P_0, and the ambient atmosphere, P_b, where the gas is discharged. The gas tank pressure is high after the loading of gaseous propellant

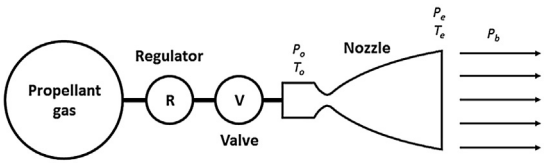

FIGURE 2.1

Schematic of a typical cold gas propulsion system.

Space Micropropulsion for Nanosatellites. https://doi.org/10.1016/B978-0-12-819037-1.00006-2

and reduces over time as it is consumed. If a stable and constant thrust is required, a pressure regulator is installed to stabilize the pressure of gas flowing out from the propellant tank to yield a consistent pressure difference.

Some possible gaseous propellants considered for early cold gas propulsion systems and their properties are listed in Table 2.1. While the use of hydrogen and helium gas as propellants provides higher specific impulses, the low density of these gases requires a large and heavy storage tank, which neutralizes the advantage in performance. On the other end of the spectrum, the heavier gas, such as Argon and Krypton, has low specific impulse. In some cases, these gaseous propellants are heated to improve the specific impulse or reduce the tank size, at the expense of a more complex design.

Cold gas propulsion with low system complexity is ideal for missions with relatively simple propulsive requirements. The simplicity of the system reduces the failure risk significantly as well, making it suitable for missions that require a robust and reliable propulsive system. Another advantage of cold gas propulsion is the free from contamination issue as a result of using inert and benign gaseous propellant. This is particularly important for missions that carry instruments, such as sensitive optical payload and mirrors, with stringent requirements on particle deposition and contamination.

Valve leakage remains the major limitation and concern for a cold gas propulsion system. Before the gaseous propellants flow into the valve, they must be adequately filtered to remove any microscopic contaminants, which could deposit on the valve seat, creating small voids where the leakage occurs. While the voids could be extremely small and not significant for liquid propellant-based systems, it is catastrophic for cold gas propulsion systems where the propellant viscosity is low and the pressure is high. In practice, an additional propellant of approximately 20% is normally filled into the tank as a design margin to compensate for potential leakage.

While cold gas propulsion has a rich heritage, most of the systems were not initially designed for nanosatellite applications. Although propellant tank and nozzle could be conveniently miniaturized according to the available volume and mass of a

Table 2.1 Properties of selected propellants for cold gas propulsion system [1].

Propellant	Molecular mass	Density[a] (lb/ft^3)	k	Theoretical specific impulse[b] (s)
Hydrogen	2.0	1.77	1.40	284
Helium	4.0	3.54	1.67	179
Nitrogen	28.0	24.7	1.40	76
Air	28.9	25.5	1.40	74
Argon	39.9	35.3	1.67	57
Krypton	83.8	74.1	1.63	50

[a] *At 5000 psia and 20°C.*
[b] *In vacuum with a nozzle area ratio of 50:1 and temperature of 20°C.*

nanosatellite, the valve requires further research and development. Conventional valve actuation consumes notably high electrical power, in the order of 1 W for holding and as high as 10 W for opening [2], which exceeds the power rating of most nanosatellites.

Typically, cold gas propulsion system produces considerably higher thrust, which is desirable for rapid orbital maneuvers, than electric propulsion systems. However, the specific impulse is rather low, less than 100 s. Considering the limited volume in nanosatellites to integrate large storage tanks, the total impulse is insufficient for high ΔV maneuvers. This limits their applications in nanosatellites primarily as an attitude control system. In addition, the leakage issue also hinders the cold gas propulsion system from implementing in long-duration missions.

2.2 Nozzle theory

Other than the hardware, that is, propellant tank, pressure regulator, and valve, the performance of a cold gas propulsion system is closely related to the design of the nozzle. Thus, the knowledge in ideal nozzle theory, which simplifies the real nozzle flow into a quasi-one-dimensional (1D) nozzle flow, is crucial for a preliminary estimation of the thruster performance. Under the ideal 1D nozzle flow condition, the following assumptions are made:

1. The working fluid is homogeneous.
2. The working fluid is gaseous. Condensed phases might exist but they are minimal and thus negligible.
3. Perfect gas law is valid.
4. There is no heat transfer across the solid boundary, that is, the flow is adiabatic.
5. The solid boundary is smooth and therefore frictional and boundary layer effects are negligible.
6. Shock wave or flow discontinuities do not occur in the nozzle flow.
7. The flow is steady, and the transient effect is negligible.
8. Exhaust gases leave the nozzle in the axial direction only.
9. Gas properties, for example, velocity, pressure, temperature, and density, are uniform in a normal cross-section of the nozzle flow.
10. Chemical equilibrium is established, that is, frozen flow.

Ideal nozzle theory applies to all chemical propulsion systems, which use a CD nozzle to accelerate the working fluid. Although cold gas propulsion is often categorized as chemical propulsion, no chemical reaction occurs. Thus, the gaseous propellant, after flowing through the opening valve, enters the nozzle as a gas phase only. Therefore, assumptions 1, 2, and 3 in the ideal nozzle theory are all valid.

Collectively, assumptions 4, 5, and 6 allow the use of isentropic relations on the nozzle flow, which is idealized as adiabatic and thermodynamically reversible. Practically, the cold gas microthruster employs a much smaller nozzle. Thus, the

assumptions shall be revised and corrected to reflect the effects of miniaturization, that is, enhanced heat loss and frictional loss at the microscale, on thruster performance.

Essentially, a CD nozzle in cold gas propulsion converts internal energy of the gas stored at high pressure of P_0 and temperature of T_0, through an isentropic gas expansion process, into kinetic energy. The gas pressure and temperature drop while the gas velocity increases to Mach number, $M = 1$ at nozzle throat and expands further to supersonic flow in the diverging section.

The total thrust produced by the nozzle flow is the sum of momentum thrust and pressure thrust that originates from the difference between the pressure at nozzle exit and ambient (back) pressure. The thrust produced is thus given by

$$F = \dot{m}V_e + (P_e - P_b)A_e \tag{2.1}$$

where A_e is the area at the nozzle exit. If the backpressure, P_b, is matching the exit pressure, P_e, optimum design condition is achieved. The thrust produced is at maximum and is a function of gas mass flow rate, $\dot{m}$, and exit velocity, V_e, only, which can be determined using

$$V_e = \sqrt{\frac{2k}{k-1}RT_0\left[1 - \left(\frac{P_e}{P_0}\right)^{(k-1)/k}\right]} \tag{2.2}$$

where k is the specific heats ratio and R is the gas constant.

The mass flow through the nozzle is a function of the throat area, A_t, and chamber pressure, P_0, and it is given by

$$\dot{m} = A_t P_0 k \frac{\sqrt{\left(\frac{2}{k+1}\right)^{(k+1)/(k-1)}}}{\sqrt{kRT_0}} \tag{2.3}$$

Specific impulse is an important performance indicator used to measure the effectiveness of a propulsion system in consuming the propellant to produce thrust. It is defined as follows:

$$I_{sp} = \frac{F}{\dot{m}g} \tag{2.4}$$

A high specific impulse implies that the propulsion system consumes less amount to propellant to produce a specific amount of thrust. This is the reason for adding thermal energy into the gas propellant via heating to reduce the mass flow rate, according to Eq. (3.3), thus increasing the specific impulse.

2.3 Selection of propellant

The choice of a suitable propellant is crucial in the development of a cold gas microthruster. The design considerations are highly dependent on the selected propellant.

The associated design solutions, such as sizing of the propellant storage tank, total impulse, thrust level, duty cycle, and maneuver duration, for a cold gas microthruster using one specific propellant, could be vastly different from the others.

The physical and chemical properties of a few propellants selected for cold gas microthruster are summarized and given in Table 2.2.

Inert gases, which do not undergo undesired chemical reactions, are among the first propellants selected to facilitate the safety issue. Nitrogen (N_2) and argon (Ar) gas are suitable candidates due to their inert nature as well as the well-established handling protocol and process inherited from various industries. Although butane is an organic compound and classified as a hazard, it has been selected as a propellant in previous missions due to its rich heritage in the past decades [3].

Depending on the mission requirements, there are different criteria for the selection of propellant. From Newton's laws of motion, the thrust produced by a cold gas microthruster is proportional to the mass flow rate of the gas expelled from the micronozzle. Thus, propellant with high molecular weight, such as xenon (Xe), is desirable for a mission that requires a high thrust level.

Ideally, the selected propellant is compressible into a liquid to save the inherently limited spatial volume in a nanosatellite. To this end, the propellant with high liquid density is favored as it maximizes the amount of propellant stored in the storage tank. The increased amount of propellant that a nanosatellite can carry into space extends the mission lifetime as the microthruster can operate for a longer duration.

It is beneficial for a propellant to possess the self-pressurization capability, which simplifies the design of subsystems. A dedicated pressurization system could be omitted to save not only the system mass and volume but also eliminate the proneness to pump failure or leakage in the connecting pipeline. For this criteria, propellant with low critical temperature is preferred so that the vapor pressure remains sufficient for effective self-pressurization in the operational temperature range of

Table 2.2 Physical and chemical properties of commonly selected propellant for cold gas microthruster.

	Molecular weight (g/mol)	Liquid density (g/cm^3)	Heat of vaporization (kJ/mol)	Critical temperature (°C)	Freezing point (°C)
Xe	131.3	3.100	12.64	16.6	−118.8
N_2	28	0.807	2.79	−146.9	−210
Ar	39.9	1.394	6.5	−122.4	−189.4
Butane	58.1	0.599	22.44	152.2	−138
SF_6	146.1	1.329	9.64	45.6	−64
R134	102	1.225	22.15	101.1	−96.7
R236fa	152	1.373	24.38	124.9	−103

the microthruster. Nevertheless, it is noteworthy that propellant with excessively low critical temperature yields high vapor pressure when the propellant is exposed to high temperature. Under this circumstance, a propellant storage tank with a thicker tank wall, thus heavier, is necessary to avoid the over-pressurization, which could be detrimental in the event of a rupture.

Owing to the limited volume available in nanosatellites, any strategy to optimize the usage of volume is highly encouraged. Compatibility of the propellant with control and power electronics offers a possibility to pack those electronic components inside the tank, which frees up more volume in exchange for additional propellant mass. Moreover, the waste heat from the electronics could be harvested to facilitate the generation of additional vapor pressure. Therefore, the propellants from the inert and noncombustible gas category are favorable.

The temperature surrounding the nanosatellite could drop rapidly beyond 0°C when the nanosatellite is at the eclipse region. Hence, the selected propellant must have a low freezing point, which could eliminate or reduce the consumption of electrical power for active thermal control.

Sulfur hexafluoride (SF_6), a nonflammable, odorless, and nontoxic gas, is commonly used as dielectric gas in the electrical industry. It is considered as a competent propellant candidate for cold gas microthruster owing to its high molecular weight and relatively high liquid density as well as the low critical temperature at 45.6°C with good self-pressurization capacity. However, it is evaluated as one of the most potent greenhouse gases, making it a less "green" candidate.

In searching for the next generation propellant, commercial refrigerants, such as R132a and R236fa, have attracted much attention recently [4,5]. Advantages of these refrigerants, such as favorable thermodynamic properties, nontoxic, compatible with most electrical and mechanical components, and high liquid density, are appealing for application in cold gas microthruster.

In certain circumstances, there are some special requirements to meet when selecting the propellant. For instance, the deployment of CubeSats from the International Space Station (ISS) has become more common. To comply with the safety regulation in ISS, the propellant used shall be nontoxic and nonhazardous. For this purpose, R236fa is the ideal candidate as it is benign and, more importantly, it can be removed from the air by the filtration system of ISS [6].

2.4 State of the art—system with flight heritage

Cold gas systems are the most mature and established propulsion technology due to their low complexity, inexpensiveness, and robustness. Thus, it is not unexpected that they are among the first propulsion technologies successfully miniaturized for nanosatellite applications. A summary of cold gas microthruster system with flight heritage is compiled and presented in Table 2.3.

Table 2.3 Summary of cold gas microthruster system with flight heritage.

Gas	Manufacturer	Thrust (mN)	Mission	Satellite mass (kg)	Year	Reference
Butane	SSTL	65	SNAP-1	6.5	2000	[7,8]
Xenon	Aerospace corporation	20	MEPSI-1	1.4	2006	[9]
SF_6	SFL	50	CanX-2	3.5	2008	[10,11]
N_2	NanoSpace	0.1—1	PRISMA	145	2010	[12,13]
N_2	TNO, U. Twente, and TU Delft	6	Delfi-n3xt	3.5	2013	[14]
SF_6	SFL	12.5—50	CanX-4/5	1.5	2014	[15]
Ar	Microspace Rapid Pte Ltd	1	POPSAT-HIP1	3.3	2014	[16]
Butane	NanoSpace	1	TW-1A	3.5	2015	[17]
R236fa	University of Texas at Austin	110	BEVO-2	3.5	2016	[18]
R236fa	VACCO	10	NanoACE	5.2	2017	[19]
Butane	NanoSpace	1	GomX-4B	8	2018	[20]
R236fa	VACCO	25	MarCO	13.5	2018	[19]
R236fa	University of Texas at Austin	110	ARMADILLO	4	2019	[18]

2.4.1 SNAP-1 (SSTL)

The first flight record of a cold gas microthruster system can be traced back to as early as 2000. Surrey Satellite Technology Ltd. (SSTL) has initiated its first nano-satellite, SNAP-1, in 1999 with the mission as an inspection satellite to capture the image of another satellite, Tsinghua-1. A single-axis propulsion system, placed as close to the satellite's center of gravity as possible, was required to propel the SNAP-1 into a close range of distance to the target satellite.

The SNAP-1 satellite bus consists of three sets of electronic modules, connected in a triangular configuration. The payload panel is placed on top of the modules, which limits the implementation of the typical design configuration of a single central propellant tank. As a result, a unique design, which removed the entire propellant tank and replaced it with a 1.1 m of coiled titanium tube, has been adapted, as shown in Fig. 2.2 [21]. This innovative pipework assembly of 65 cm^3 volume is possible due to the selection of butane as a propellant.

Five possible propellants were considered. While nitrogen and Xenon gas provide the most inferior performance, the need for a heavy high pressurized tank has ruled them out, considering the total mass of the satellite is merely 6.5 kg. Of

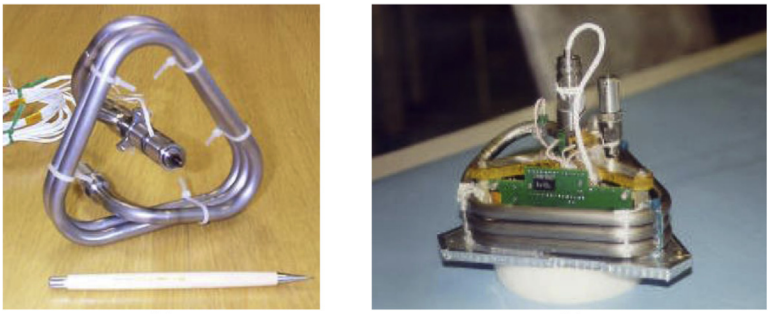

FIGURE 2.2

(A) Pipework assembly and (B) integrated cold gas propulsion module of SNAP-1.

Reprint with permission from Chapter 8 - Micropropulsion, in: Z. You (Ed.), Space Microsystems and Micro/Nano Satellites, 2018, Butterworth-Heinemann. pp. 295–339.

the three remaining options, ammonia outperforms propane and butane in terms of total impulse. Safety concerns arose as ammonia is a toxic substance, which requires special handling and hence additional cost. Eventually, butane was chosen due to its lower vapor pressure of 3.8 bar (as opposed to 14.5 bar for propane) at the operating temperature of 40°C. The low pressure provides a good safety margin of 200 for titanium tube and 12 for isolation valve, respectively.

The pipework assembly is connected to a fill valve on one end for filling of butane propellant while a thruster valve on the other end for operational control. An isolation valve is placed in between them to protect against a thruster leakage. The integrated propulsion module, with a total mass of 450 g including 32.6 g of butane, is shown in Fig. 2.2B. The system has successfully been tested in space and raised the orbit of SNAP-1 by 2.6 km. The specific impulse achieved is evaluated as 43 s, which is lower than the theoretical value of 70 s, due to incomplete vaporization of butane that led to the expulsion of liquid phase propellant at the early stage of operation. Nevertheless, the targeted total ΔV of 2 m/s was achieved.

2.4.2 MEPSI (The Aerospace Corporation)

Microelectromechanical system (MEMS) PICOSAT Inspector (MEPSI) mission consists of a tethered pair of picosatellites. After ejection from the Space Shuttle Discovery during the STS-116 mission, the two picosatellites were separated by a tether of 15 feet, which keeps them floating apart. One picosat (Inspector) uses its cold gas propulsion system, developed by The Aerospace Corporation, to get closer to the other picosat (Target) for inspection and download the imagery to the earth ground station.

In any cold gas propulsion system, a pipeline connects one component to the other, for example, propellant tank to valve. The joints, where the pipeline interfaces with the component, are the points for potential leakage if not properly welded. The issue is particularly alarming as welding could be challenging given the very small and limited volume available in picosatellite. The Aerospace Corporation team used stereolithography (SLA) additive manufacturing technology to produce a leak-tight manifold, which includes tanks, plumbing, and nozzle, in one piece, eliminating the distinct joints except the valve connection, as shown in Fig. 2.3.

The fully integrated cold gas propulsion system has five (5) thrusters rated at 20 mN each, uses xenon gas as a propellant, $1 \times 3.6 \times 3.6$ in. in dimension, and weighs 188 g. The system fabricated using Somos 11120 polymeric material was tested to 1000 psi without breaking, which fulfills the requirement by NASA of 2.5 times the maximum design pressure of 115 psig. Another concern with the use of polymeric material in outer space is the outgassing. The Somos 11120 material was sent for outgassing tests, which reported a relatively large total mass loss (TML) of 2.85% and an acceptable collected volatile condensable mass of 0.01%. Additional procedures to heat the SLA-printed manifold to 60°C in a vacuum for 12 h were carried out to remove the volatile elements and hence lower the TML.

The nozzle A in MEPSI cold gas system was operated on orbit as confirmed by the picosatellite rotation rates measured using the onboard triaxial rate sensor. The impulse of 2.6×10^{-3} Ns was evaluated based on the consumption of 0.2 cc xenon gas discharged at 115 psia and a specific impulse of 30 s. However, the mission was short lived as the picosatellites encountered a memory overflow condition after the operator has put them to sleep over the Christmas holiday in 2006. The flight computer went into an infinite loop and the picosatellites never awoke.

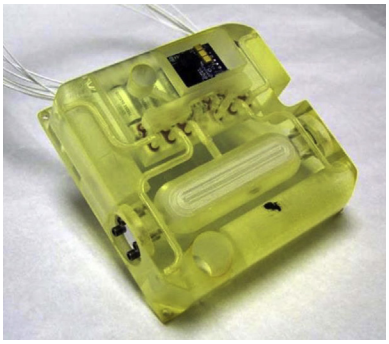

FIGURE 2.3

Leak tight manifolds fabricated using SLA additive manufacturing technology.

Reprint with permission from K. Lemmer, Propulsion for CubeSats, Acta Astronaut. 134 (2017) 231–243.

2.4.3 CanX-2 and CanX-4/5 (UTIAS/SFL)

Canadian Advanced Nanospace eXperiment 2 (CanX-2) is a 3U CubeSat of 10 × 10 × 34 cm with a mass of 3.5 kg, developed by the University of Toronto, Institute for Aerospace Studies, Space Flight Laboratory (UTIAS/SFL). CanX-2 serves as a precursory mission to develop and test several enabling technologies for the upcoming CanX-4/5 formation flying mission.

One of the key technologies demonstrated in the CanX-2 mission is Nanosatellite Propulsion System (NanoPS), as shown in Fig. 2.4 [23]. It is a cold gas microthruster system, using sulfur hexafluoride (SF_6) as a propellant. The system is 500 g in weight and provides a thrust of 50 mN with a specific impulse of 50 s. It is designed mainly for attitude control maneuvers. Thus, the nozzle is positioned such that the thrust produced by NanoPS induces a major-axis spin on the nanosatellite. CanX-2 was launched into space in 2008. After 1 year of operation, it has met and exceeded all mission objectives.

CanX-4/5 is a dual-nanosatellite formation flying demonstration mission. To achieve and maintain a precise satellite formation, precise relative position determination and accurate thrusting are required. Based on the NanoPS heritage on CanX-2, UTIAS/SFL has built Canadian Nanosatellite Advanced Propulsion System (CNAPS) for CanX-4/5, a pair of two identical nanosatellites of 1.5 kg each.

Similar to NanoPS, CNAPS uses SF_6 as a propellant and is able to achieve a specific impulse of 45 s. Loaded with a propellant capacity of 260 mL, CNAPS is capable of a total ΔV of 18 m/s. It is equipped with four (4) independently controlled thrusters located on one face of the nanosatellite bus, with a combined thrust level in the range of 12.5−50 mN, depending on the chamber pressure. As the thrusters are configured to offset from the center of mass, each thruster can be operated independently and used for momentum management in reducing the build-up of unwanted torque.

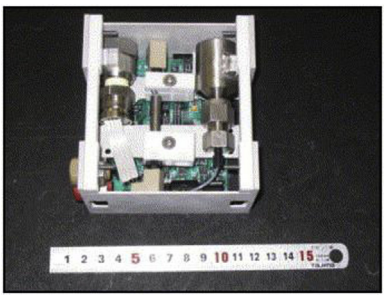

FIGURE 2.4

Nanosatellite Propulsion System (NanoPS) payload for CanX-2 mission.

Reprint with permission from K. Sarda, et al., Canadian advanced nanospace experiment 2: scientific and technological innovation on a three-kilogram satellite, Acta Astronaut. 59 (1) (2006) 236–245.

The twin nanosatellites were launched in 2014 onboard the Polar Satellite Launch Vehicle, from India. CNAPS has been successfully used to perform a series of precise, controlled, and autonomous formation flights from 1 km range down to 50 m separation between the two nanosatellites.

2.4.4 Delfi-n3xt (TNO, U. Twente, and TU Delft)

The Delfi-n3Xt is a 3U CubeSat, developed under the Delfi program by the Delft University of Technology (TU Delft). One of its mission objectives is to prequalify the $T^3\mu PS$, a cold gas micropropulsion system jointly developed by TNO, TU Delft, University of Twente and SystematIC Design BV. MEMS technology has been used extensively to develop an integrated propulsion system of valve, nozzle, pressure transducer, and filter, as schematically shown in Fig. 2.5.

An innovative way to store the gaseous propellant in a form of solidified grain has been developed. Upon heating the solid grain (Fig. 2.6A) in the Cold Gas Generator (CGG), nitrogen gas is released and flows into a plenum for pressurization. The thrust of up to 6 mN can be produced by opening the valve for the compressed gas to exit from the nozzle. The flight model of $T^3\mu PS$, weights 120 g, is shown in Fig. 2.6B.

The system has been tested in orbit shortly after the launch in 2008. Two out of six CGGs were successfully ignited using 10.1 and 10.3 W of electrical power, respectively, before the failure in the ignition train. A spike in the plenum pressure confirms the release of nitrogen gas from the solid grain. A drop in pressure transducer reading after the valve was opened affirms the thrust generation.

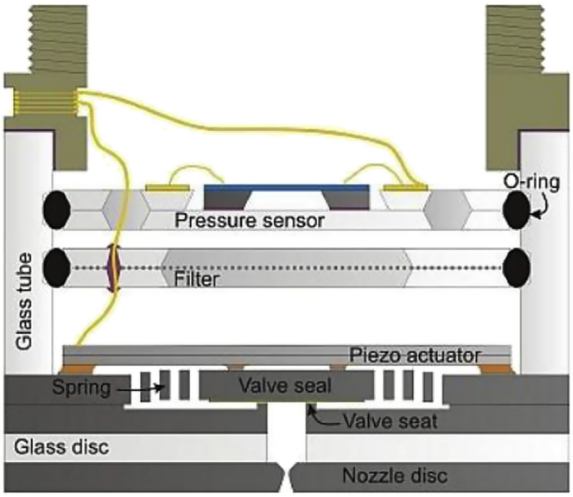

FIGURE 2.5

Schematic of cold gas micropropulsion system in Delfi-n3xt nanosatellite.

Reprint with permission from Delfi Space.

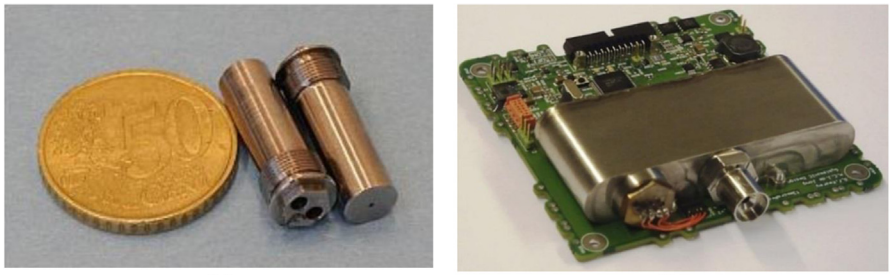

(a) (b)

FIGURE 2.6

(A) CGG used to produce nitrogen gas; (B) flight model of $T^3\mu PS$.

Reprint with permission from Delfi Space.

2.4.5 POPSAT-HIP1 (microspace)

Propulsion Operation Proof SATellite-High Performance 1 (POPSAT-HIP1) is a 3U CubeSat of 3.3 kg in mass, developed by Microspace Rapid Pte Ltd. It features a cold gas micropropulsion system for attitude control with eight (8) micronozzle modules, as shown in Fig. 2.7A. The supersonic micronozzle structures are mass-produced using a series of silicon MEMS microfabrication techniques, that is, microlithography, deep reaction ion etching, and anodic bonding. After dicing the silicon wafer, an individual micronozzle chip is produced (Fig. 2.7B). Using 5 bar of Argon gas as propellant, each micronozzle chip can produce a nominal thrust of 1 mN.

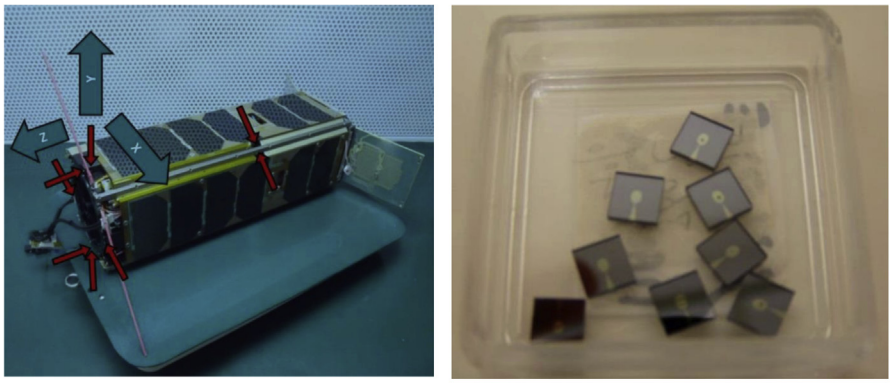

(a) (b)

FIGURE 2.7

(A) Position of eight micronozzle modules as pointed out by *red arrows*; (B) individual silicon micronozzle chip after dicing.

Reprint with permission from MicroSpace Pte Ltd.

The CubeSat was launched into orbit in 2014. Performance of the cold gas micropropulsion system in angular velocity change, detumble, reduction of angular velocity, and attitude change along two axes has been demonstrated. Maneuvers of 4 degrees/s and up to 10 degrees/s were achieved with the tank pressure of 2 and 5 bar, respectively. During the 9 months in orbit, the system was able to produce a total ΔV up to 3 m/s.

2.4.6 PRISMA, TW-1A and GomX-4B (NanoSpace)

Prototype Research Instruments and Space Mission technology Advancement (PRISMA) is a formation flying and rendezvous technologies demonstration mission, led by Swedish Space Corporation. It consists of two spacecraft. The MAIN spacecraft is highly maneuverable, equipped with three different types of propulsion systems, and hence capable of performing a series of maneuvers around the smaller TARGET spacecraft.

The MAIN spacecraft uses the conventional hydrazine reaction control system, with ΔV capacity of 120 m/s, for most of the maneuvers. Simultaneously, another two propulsion systems, that is, high-performance green propulsion and MEMS-based cold gas micropropulsion, were included as a technology demonstration.

While PRISMA, weighing 145 kg, is not in the nanosatellite category, it has successfully flight demonstrated the functionality and performance of the first fully integrated cold gas micropropulsion system developed by NanoSpace using MEMS technology. The thruster pod consists of a silicon wafer stack with four (4) micromachined microthrusters and integrated with MEMS-based flow control valves, filters, and heaters (Fig. 2.8). Each thruster is capable of producing thrust in the range of 10 μN to 1 mN, using nitrogen gas as a propellant. It is noteworthy that the use of MEMS technology has not only miniaturized the size of the system significantly but also reduced the power consumption of the valve to 3 W per thruster, which is within the power budget of a nanosatellite.

Following the successful technology demonstration in the PRISMA mission, NanoSpace has developed a MEMS-based cold gas micropropulsion system for 3U CubeSat, named as NanoProp CGP3 (Fig. 2.9). The system occupies 0.5 U of volume, uses butane gas as a propellant, and weighs only 350 g (wet mass). There are four (4) individual thrusters, producing 1 mN of thrust each and thrust resolution as low as 10 μN, suitable for both translational maneuvers and attitude control. It has been flight proven and used in formation flying demonstration in TW-1A, a 3U CubeSat developed by Shanghai Engineering Center for Microsatellites, in 2015.

The development of MEMS-based cold gas micropropulsion system for nanosatellites in NanoSpace continues, the first cold gas propulsion system compatible with 6U CubeSat has been developed. The system shares some similarities, such as butane gas as a propellant, four (4) individual thrusters, and 1 mN thrust for each thruster, with NanoProp CGP3 to capitalize on the rich heritage from previous missions. It occupies a volume of 200 × 100 × 50 mm and weighs 900 g (wet mass). The two tanks configuration provides additional redundancy to the system.

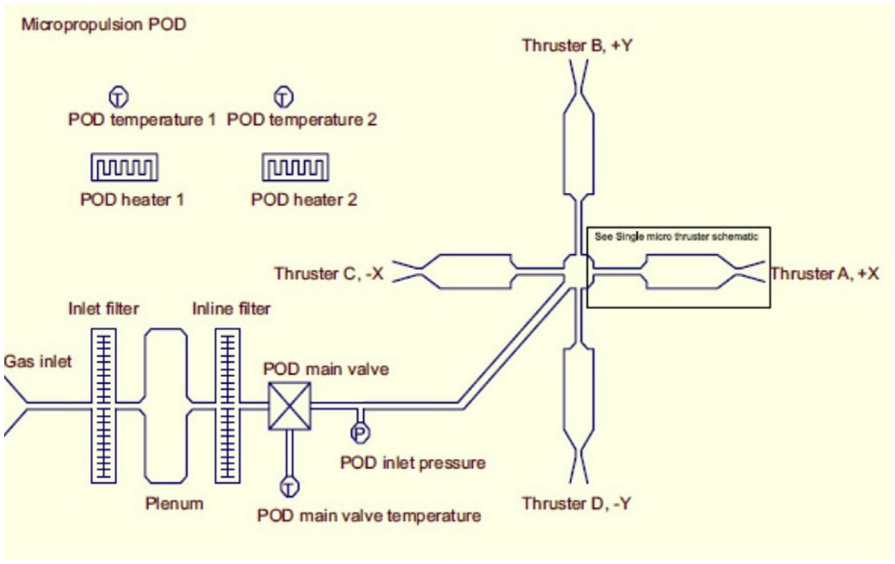

FIGURE 2.8

(A) Schematic of MEMS-based micropropulsion system developed by NanoSpace; (B) thruster pod assembly, 44 mm in diameter and 51 mm in height.

Reprint with permission from T.-A. Grönland, et al., Miniaturization of components and systems for space using MEMS-technology. Acta Astronaut. 61 (1) (2007) 228–233.

The system, named as NanoProp 6U, has been flight proven in the GomX-4 mission in 2018. The mission consists of two 6U CubeSats, GomX-4A and GomX-4B, to demonstrate the key technologies required for large satellite

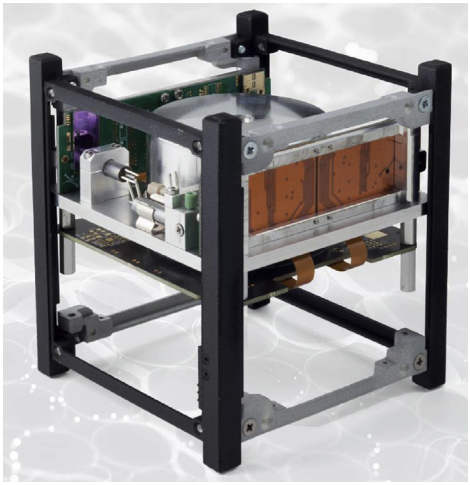

FIGURE 2.9

NanoProp CGP3 cold gas micropropulsion system developed by NanoSpace for 3U CubeSat [22].

formations in the future. Only GomX-4B is equipped with the propulsion system to perform a critical maneuver, which increases the separation distance between the two nanosatellites to 4500 km, a critical distance set by Earth's curvature, to carry out the intersatellite radio link experiments.

2.4.7 NanoACE and MarCO (VACCO)

VACCO Industries, a company with more than 60 years of experience in engineering and manufacturing of various fluid control components for space applications, has developed a few cold gas micropropulsion systems, specifically for CubeSats. It has supplied its latest Reaction Control Propulsion Module to Tyvak Nanosatellite System Inc for a 3U CubeSat mission, NanoACE. The mission is an internal development program of Tyvak to validate technologies that will be used in future missions.

The module is a self-contained unit and occupies the center of the 3U CubeSat. It has a total of eight (8) thrusters located at the four corners for rendezvous and proximity operations. Each thruster is designed to produce 25 mN of nominal thrust using R236fa as a propellant. The system has been flight proven in 2017.

VACCO has also developed a smart, self-contained micropropulsion system (MiPS) for the first interplanetary CubeSats, Mars Cube One (MarCO). The mission consists of two 6U CubeSats to function as a communication relay for the InSight lander.

The two experimental CubeSats were launched in 2018. After 7 months of cruising together with InSight lander, they survived the trip to deep space. However, the twin CubeSats were last contacted on December 29, 2018. Since then, the engineers have lost communication with the CubeSats. No experiments are conducted for the MiPS system, which has four (4) thrusters with 25 mN nominal thrust, using R236fa as a propellant and a designed total impulse of 775 Ns.

2.4.8 BEVO-2 and ARMADILLO (University of Texas at Austin)

The University of Texas at Austin's Satellite Design Lab has developed a cold gas micropropulsion system for Bevo-2, a 3U CubeSat. The system was manufactured using additive manufacturing technique, SLA, which allows the propellant tank, secondary tanks, internal piping, and nozzle encased in a single block.

The system uses R236fa as a propellant, which is stored in the main tank and flow into the plenums for a complete expansion to gases before exhausting to vacuum space through the nozzle (Fig. 2.10). The thruster is producing thrust in the range of 110−150 mN for a temperature range of 24−85°C. The total mass of the system is 400 g, including 90 g of propellant.

According to the mission planning, the Bevo-2 was scheduled to deploy together with another bigger nanosatellite, AggieSat-4, of 50 kg from ISS in 2016. After the deployment, they will separate in orbit. A proximity operation will be executed thereafter. Unfortunately, the BEVO-2 CubeSat experienced a communication issue and was not activated.

The same cold gas micropropulsion system (Fig. 2.11) was selected in the early stage of another 3U CubeSat mission, ARMADILLO, by the University of Texas at Austin in collaboration with Baylor University.

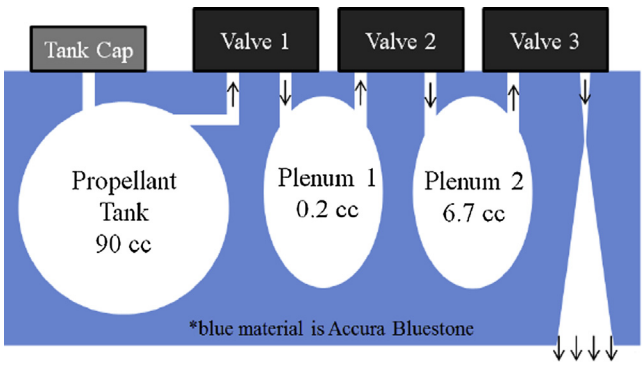

FIGURE 2.10

Schematic of thruster design.

Reproduce with permission from S. Wu, et al., TW-1: a cubesat constellation for space networking experiments. in: 6th European CubeSat Symposium, 2014.

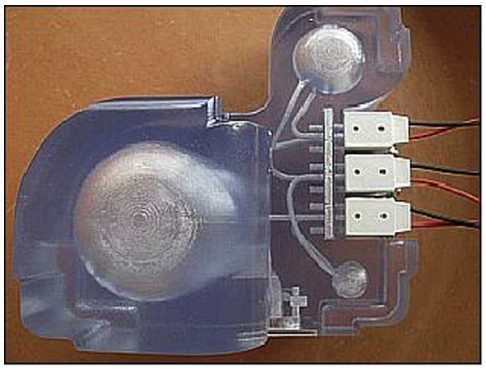

FIGURE 2.11

Cold gas micropropulsion system featured in Bevo-2 and ARMADILLO CubeSats.

Reproduce with permission from Texas Spacecraft Laboratory.

2.5 Challenges and future

Other than the aforementioned systems that had successfully flight proven, we expect to see more cold gas micropropulsion systems adopted in a wide range of space missions with a scheduled launch in 2019 and 2020. Some of the examples are listed in Table 2.4.

Because of the use of its proprietary Chemically Etched Micro Systems (ChEMS) fabrication technique, cold gas micropropulsion systems from VACCO are generally producing thrust in the range of 10–25 mN. Coupled with its rich heritage and expertise in feed systems, valves, and propellant storage tanks, VACCO's cold gas micropropulsion systems are robust and reliable, particularly suitable for

Table 2.4 Summary of future missions with cold gas micropropulsion system.

Gas	Manufacturer	Thrust (mN)	Mission	Satellite	Expected launch	Reference
R236fa	VACCO	25	CuSP	6U CubeSat	2019	[19]
R236fa	VACCO	25	Omotenashi	6U CubeSat	2019	[19]
R134a/ ADN	VACCO	25	ArgoMoon	6U CubeSat	2019	[19]
R236fa	VACCO	10	CPOD	3U CubeSat	2020	[19]
R236fa	VACCO	25	NEA Scout	6U CubeSat	2020	[19]
R236fa	Georgia Institute of Technology	50	BioSentinel	6U CubeSat	2020	[24]

high-value future missions of 3 and 6U CubeSats. NanoSpace is another company that offers matured and flight-proven cold gas micropropulsion systems. Differ from VACCO's systems, NanoSpace is using MEMS microfabrication techniques, which are able to produce nozzle with dimensions in the order of tenths of micrometers. Thus, the thrust level of NanoSpace's systems can be as low as 1 mN.

While the cold gas micropropulsion systems from both companies are highly integrated and matured, the unit cost might not be affordable for some first-time CubeSat missions by universities, which usually have a relatively limited budget. Thus, we have also seen a few cold gas micropropulsion systems developed using 3D additive manufacturing technology, which is very cost effective. Although the material used might not be fully space qualified, it is acceptable for short missions. In addition, 3D additive manufacturing technology is rapidly developing. New manufacturing capabilities and materials will have positive impacts on the future development of cold gas micropropulsion systems based on additive manufacturing.

In the pursuit of a lower thrust level for implementation of cold gas micropropulsions systems in smaller nanosatellites as primary propulsion systems or to provide more precise attitude control capability in bigger nanosatellites, a smaller nozzle (known as micronozzle) is the key enabling component. The subsequent subsections will elaborate on the miniaturization of the nozzle using MEMS technology. Followed by some insights on the optimization of micronozzle design to address the low-performance efficiency in micronozzle.

2.5.1 Miniaturization of nozzle via MEMS approach

With volume in nanosatellites being extremely valuable, it is necessary to reduce the size of propulsion systems as much as possible. With micromachining methods such as micromilling or electrical discharge machining (EDM) methods, one is able to generate features as small as a few hundred microns. However, would one want to further reduce the size of the various propulsion subsystems, alternative manufacturing methods are required. For this further reduction in size, MEMS manufacturing techniques meet the requirements and are generally used in mircopropulsion.

The manufacturing techniques applied for MEMS systems are the same as those used for the semiconductor industry. The smallest attainable feature size is a few nanometers but is rapidly changing, as the semiconductor industry is ever pushing the boundaries to manufacture smaller transistors to keep up with Moore's law. While MEMS manufacturing techniques allow for further reduction of the propulsion system size, they also generate additional limitations. Firstly, the selection of materials is limited as most MEMS manufacturing techniques are designed around the usage of silicon or its derivatives. Although there are some studies that use ceramic as structural materials [25,26], this may not offer an obvious advantage for cold gas micropropulsion systems as they are not operating at high temperatures.

Most micropropulsion systems built with MEMS manufacturing techniques utilize deep reactive ion etching (DRIE). DRIE is a highly anisotropic etching

method that is able to generate features with extremely high aspect ratios. DRIE obtains this by alternating between two processes: a short isotropic plasma etch and the deposition of a passivation layer. In the isotropic plasma etch, a plasma, which is made of an appropriate etchant gas, is shot/accelerated perpendicular to the top of the wafer. The ions and free radicals will chemically react on the surface of the wafer and isotropically etch the material away. To generate a useable shape during this etching step a so-called "mask is applied on the top side prior to the DRIE process. This "mask" is a thin deposited layer on top of the wafer with the to be etched shape, e.g., the microthruster, etched out of it. This thin deposited layer is made from a material that will not be etched by the etchant plasma used in the DRIE etch. This way one etches the desired shape into the silicon wafer during the plasma etch step of the DRIE etch. As mentioned this plasma etch step isotropically etches the material away. This would mean that the desired shape would lose all its distinction after a longer etch. As such to generate the necessary depth of the etch while still maintaining a distinctive shape the plasma etch is alternated with a passivation deposition step. This deposition step will deposit an inert material, often some form of polymer, that will prevent any further chemical etching. This adheres to the sidewalls and the bottom of the etched trench in the previous plasma etch step. In the plasma etch the accelerated ions blast away the polymer from the bottom of the trench opening the silicon substrate to the chemical plasma etch. As such one will continue to etch toward the bottom while maintaining the desired profile. This repeated usage of an isotropic plasma etch does result in so called "scallops" on the sidewalls (Fig. 2.12) [27].

Additionally, the manufacturing techniques etch a prescribed pattern into a silicon wafer in the direction perpendicular to the plane on which the pattern is described. Therefore, one is unable to generate a pattern in the etch direction.

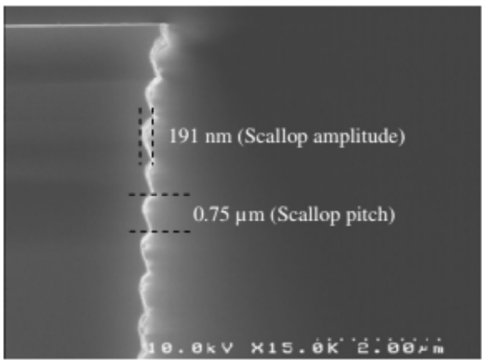

FIGURE 2.12

SEM image of DRIE etched sidewall.

Reproduce with permission from A.M. Malik, et al., Deep reactive ion etching of silicon moulds for the fabrication of diamond x-ray focusing lenses, J. Micromech. Microeng. 23 (12) (2013) 125018.

This results in micronozzles that cannot be axisymmetric: all micronozzles manufactured using MEMS techniques have a rectangular cross-section, as shown in Fig. 2.13 [28].

Various alternative MEMS manufacturing methods such as femtosecond laser machining (FLM) and micro-EDM milling are being researched to be able to manufacture axisymmetric micronozzles. Both methods show promising results to generate axisymmetric nozzles (Fig. 2.14). However, these manufacturing methods are not without drawbacks. The FLM generated geometries are experiencing a significant off-axis thrust component, which was generated due to the fact the axis was not perfectly aligned [29]. The micro-EDM method experienced quite some difficulty to achieve a smooth throat area (Fig. 2.15). Additionally, the throat sizes that one is able to achieve using this method are a multitude larger than that of more conventional methods [30]. Despite these shortcomings, the initial results of these tests show great promise and future developments could result in a shift toward these axisymmetric manufacturing methods. However, due to the wide availability of DRIE equipment, and the well-understood DRIE process, the industry's standard as of now is still DRIE manufactured nozzles with the consequent limitation of producing nozzles having rectangular features.

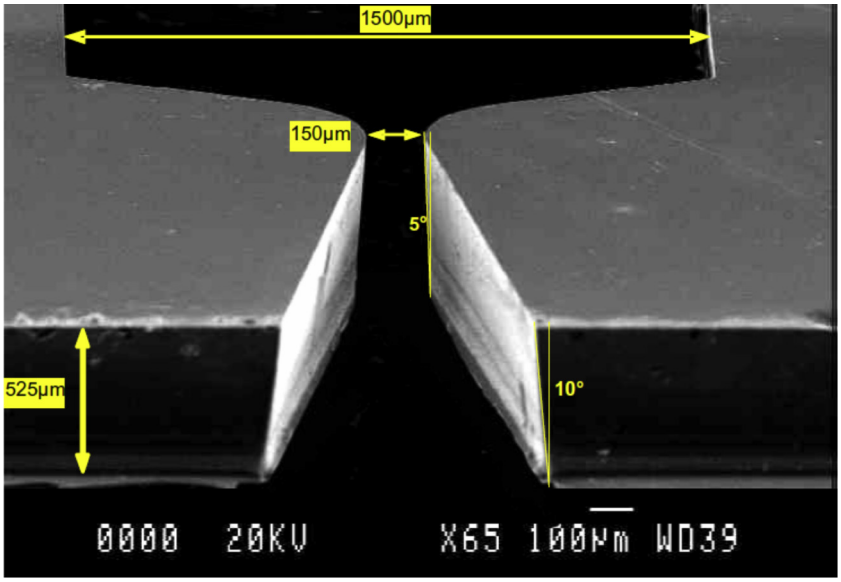

FIGURE 2.13

Rectangular cross-section of micronozzle fabricated using DRIE.

Reproduce with permission from A. Chaalane, et al., A MEMS-based solid propellant microthruster array for space and military applications, J. Phys. Conf. 660 (2015) 012137.

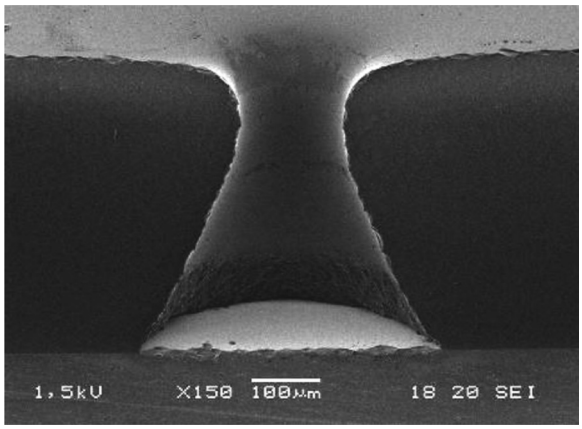

FIGURE 2.14

Axisymmetric 3D micronozzle fabricated using FLM method.

Reproduce with permission from M.C. Louwerse, et al., Nozzle fabrication for micropropulsion of a microsatellite, J. Micromech. Microeng. 19 (4) (2009) 045008.

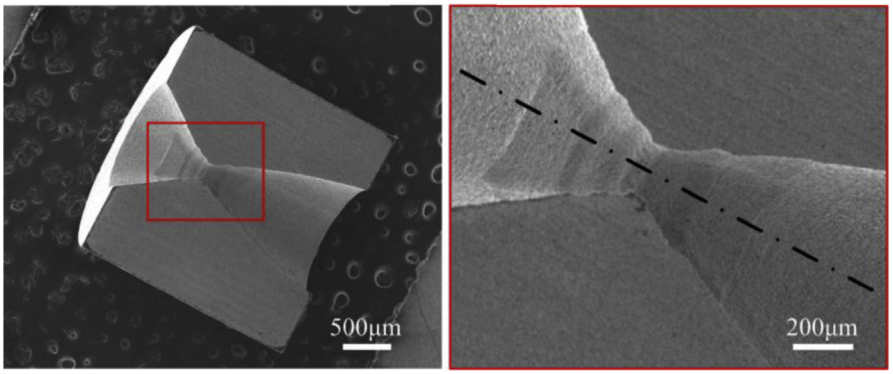

FIGURE 2.15

Axisymmetric 3D micronozzle fabricated using micro-EDM method.

Reproduce with permission from H. Li, et al., Fabrication of ZrB2–SiC–graphite ceramic micro-nozzle by micro-EDM segmented milling, J. Micromech. Microeng. 28 (10) (2018) 105022.

2.5.2 Optimization of micronozzle design

With the usage of MEMS manufacturing techniques, propulsion subsystems were reduced to extremely small sizes with the design nozzle throat being as narrow as 10 µm. With these tiny dimensions, the throat Reynolds number, which is defined by Eq. (2.5), will typically be below 10,000. This is various orders of magnitude lower than the Reynolds number encountered in conventional macro nozzles where throat Reynolds numbers exceed one million.

$$Re_t = \frac{\rho_t V_t D_t}{\mu_t} \tag{2.5}$$

Past research, both numerical and experimental, showed a staggering decrease in nozzle efficiency with decreasing throat Reynolds numbers [31,32]. Especially once the throat Reynolds numbers start to drop below 1000, the decrease in efficiency starts to accelerate, attributed to viscous losses where the thickness of the boundary layer is of importance. In conventional macro nozzles, the thickness of the boundary layer is negligible compared to the overall size of the nozzle. However, once the overall size of the micronozzle starts to decrease, the size of the boundary layer is no longer negligible. In certain cases, the boundary layer can grow to such proportions that it starts to occupy the entire nozzle cross-section (Fig. 2.16), leading to a fully subsonic flow at the divergent section of the nozzle [33]. This boundary layer constricts the effective useable nozzle cross-section and is therefore detrimental to the overall nozzle efficiency. This effect is only amplified at lower throat Reynolds numbers where the boundary layer grows in size.

Past efforts focused on mitigating these losses by using alternate geometries in the nozzle divergent [34,35]. Changing the design parameters, such as the divergence half angle and nozzle length [31,33], of conventional nozzle geometries, one is able to mitigate a significant amount of the viscous losses. However, an optimal geometry exists for each situation and ideally one would like to find this optimal design depending on the initial requirements and constraints. As manufacturing and experimentally testing the range of possible variations of nozzles would be very expensive, tedious, and difficult to perform accurately, numerical simulations are very valuable in obtaining a first-order determination of the optimum design.

However, numerical simulations are not without complications. Due to the extremely small characteristic sizes and low pressures (near-vacuum space environment at the nozzle exit) encountered in micronozzles the continuum assumption, on which most common CFD simulation tools are based, can start to break down, limiting the usability of a lot of common simulation tools. The degree to which

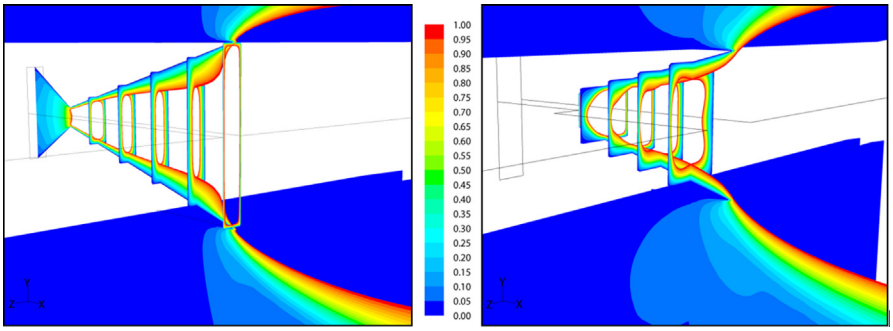

FIGURE 2.16

For $Re \sim 160$ the subsonic layers merge and the entire cross-section of the flow is subsonic. For $Re \sim 320$, only a very narrow region in the center of the flow remains supersonic.

Reproduce with permission from K.H. Cheah, J.K. Chin, Performance improvement on MEMS micropropulsion system through a novel two-depth micronozzle design, Acta Astronaut. 69 (1) (2011) 59–70.

the continuum assumption breaks down can be indicated by introducing the Knudsen number. The Knudsen number is defined by

$$Kn = \frac{\lambda}{L} = \sqrt{\frac{\gamma\pi}{2}}\,\frac{M}{Re} \tag{2.6}$$

where λ is the mean free path of a molecule, L is the characteristic length of the flow, γ is the specific heat ratio, M is the local Mach number, and Re is the local Reynolds number.

This number indicates the amount of rarefaction of a flow, a low Knudsen number ($Kn < 0.01$) is indicative of a flow where the continuum assumption is still valid [36]. However, a flow with a Knudsen number above 0.01 will start to show some rarefaction effects. This Knudsen number is inversely related to the Reynolds number, and thus higher Knudsen numbers can be expected in micronozzle flows due to the low Reynolds number.

2.5.2.1 Past developments

With the continuum assumption possibly breaking down, simulations based on the Navier–Stokes equations will start to produce less accurate results. Thus, it was proposed to simulate the flow in the micronozzle using Direct Simulation Monte Carlo (DSMC) [37]. This method is a discrete probabilistic method that simulates single particles in a volume of fluid, each representing a predetermined amount of physical molecules. Through this approach, one is able to simulate a flow for the full range of Knudsen numbers, as the simulated flow is no longer a continuous medium but rather a collection of particles. However, the computational cost of this method is orders of magnitude higher than methods utilizing the continuum assumption.

Micronozzle optimization studies require many simulations to investigate the parametric influence of a selected design parameter on the nozzle performance. This, combined with the fact that computational resources were very limited in the preinformation age era, led to most optimization studies being done using Navier–Stokes-based solvers. Additionally, these optimization studies mostly focused on 2D simulations to limit the computational cost. The validity of these simulations was still kept by utilizing nozzle backpressure that was much higher than vacuum, that is, 1000 Pa. By utilizing this higher backpressure, one ensures that the Navier–Stokes-based solver remains in a Knudsen number regime where it produces valid results [36].

This Knudsen validity regime threshold can be accurately determined through DSMC simulations and is currently a topic of hot debate in the literature. Still, by means of these former 2D Navier–Stokes-based analysis, the following important design considerations could be found:

- Angles of nozzle half divergence larger than the conventional 15 degrees deliver better-performing micronozzles at lower Reynolds numbers. For throat Reynolds numbers below 1000, half angles of 30 degrees and 45 degrees become the most commonly used, with higher angles performing better at lower Reynolds numbers [31,32,36].
- Bell nozzle profiles do not provide higher efficiencies compared to linear nozzles and therefore are not worthwhile to investigate further [34].

2.5.2.2 Current developments

In the last decade, the computational resources available to academic researchers have dramatically increased. As such, 2D numerical simulations using DSMC became more common. Minor micronozzle studies were performed using DSMC; however, large-scale optimization studies still remained too computational costly.

In addition, various efforts were made to make DSMC more computationally efficient for micronozzle simulations through the usage of a hybrid Navier-Stokes-DSMC solver. This solver would simulate the high-density regions, which are very computationally costly if performed with DSMC, using Navier−Stokes. Downstream in the micronozzle, when the pressure drops and thus the Knudsen number rises, the solver switches to DSMC. By utilizing this approach, one is able to achieve the same accuracy of DSMC with as little as 25% of the computational cost compared to a full DSMC simulation [38]. This hybrid approach has great potential for future efforts but, as of today, no optimization or design efforts are run with such a hybrid solver as most research using these solvers is on confirming their accuracy such that they can be used for future research.

However, the preference often still lies with the Navier−Stokes-based solvers for their reasonable accuracy and low computational cost. 3D numerical simulations using Navier−Stokes solvers started to become more common. These simulations found that the 3D micronozzles would significantly underperform their 2D counterpart. This was explained due to the additional losses caused by the presence of a boundary layer that grows on the end walls which previously, in 2D simulations, were neglected.

The influence of the most common design parameters, such as nozzle depth, divergence half angle, and nozzle length, started to be covered extensively given the more powerful simulation means available. Therefore, current developments start to look at novel alternative geometries to further increase the micronozzle efficiency. Examples of such alternative geometries are double-depth linear nozzles, the linear microaerospike nozzle, and double depth linear aerospike nozzles.

Double-depth linear nozzles have a sudden increase in the nozzle depth immediately after the throat. This increase in depth aims to make the boundary layer that grows on the end wall in the divergent section of the nozzle relatively of lesser importance, as it occupies less of the nozzle cross-section. Through this method, performance improvements of up to 5% were realized [33].

The aerospike design is interesting for micronozzles, not much for its ambient pressure compensation features, but more for the fact that the divergent section is an external flow body. This not only means that the flow is able to freely expand to the ambient pressure but also that the flow is not bounded in the etch direction by end walls. Therefore, due to the absence of these walls, the nozzles will also not have any related losses, which is expected to result in higher nozzle efficiencies. 2D numerical studies [35,39] showed great promise for this nozzle geometry, with it generally outperforming the linear nozzles.

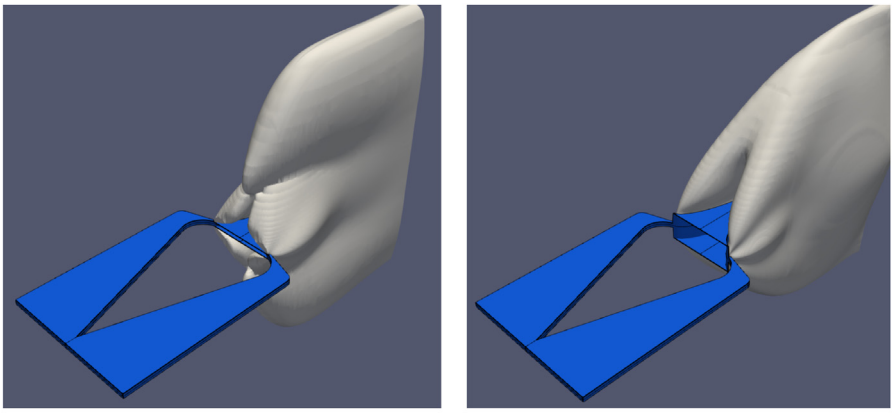

FIGURE 2.17

(A) Single depth aerospike nozzle: curling of flow expansion near the edge for $Re_t \approx 2861$. This yields excessive frictional loss. (B) Double-depth aerospike nozzle: Flow expansion over the contour for $Re_t \approx 2861$.

However, 3D numerical studies [39,40] showed that excessive losses over the edge, visible in Fig. 2.17A, cause three-dimensional aerospike designs to severely underperform compared to their two-dimensional counterparts, and in some cases even perform worse than linear nozzles.

A solution for this issue can be represented by a double-depth aerospike nozzle [40]. By increasing the depth of the center body of the aerospike, one is able to force the exiting flow to expand over a contour in contrast to curling over the edge of the center body (Fig. 2.17B). This design solution has shown great potential in 3D numerical simulations, with efficiency improvements of over 20% compared to linear nozzles (Fig. 2.18).

With the emergence of these new alternative micronozzle geometries of great potential in terms of performance and efficiency, the future of micronozzles looks bright. Furthermore, it is expected that further optimization studies on these new geometries could bring even further improvements in nozzle efficiency. Additionally, future computational advancements could make hybrid-DSMC optimization studies feasible, which would allow numerical studies to be performed with near-vacuum ambient back-pressures and, thus, closer to the actual operating conditions of these nozzles in space.

Additionally, the manufacturing techniques etch a prescribed pattern into a silicon wafer in the direction perpendicular to the plane on which the pattern is described. Therefore, one is unable to generate a pattern in the etch direction. This results in micronozzles that cannot be axisymmetric: all micronozzles manufactured using MEMS techniques have a rectangular cross-section.

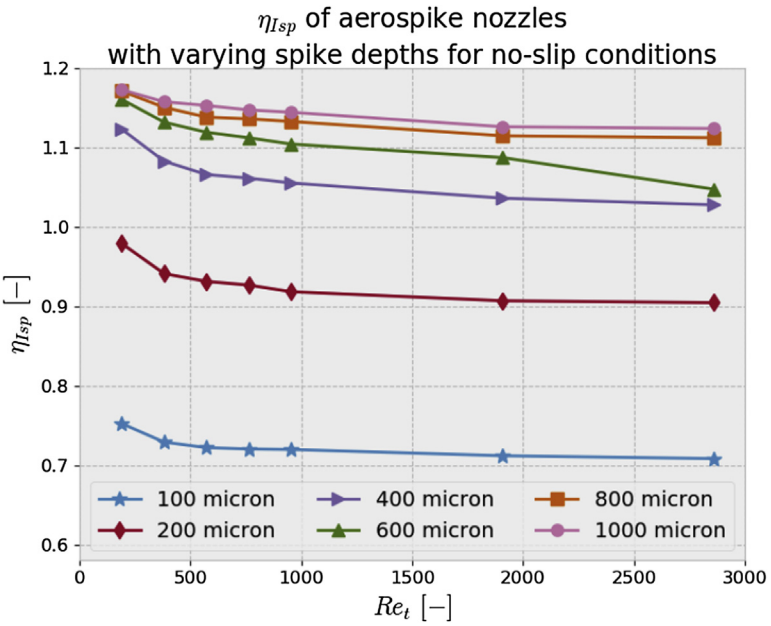

FIGURE 2.18

Specific impulse efficiency of the double depth aerospike nozzles.

References

[1] Sutton, G.P., Biblarz, O., 2001. Rocket Propulsion Elements, seventh ed. John Wiley & Sons.

[2] Mueller, J., et al., 2010. Survey of propulsion options for cubesats. In: 57th JANNAF Propulsion Meeting.

[3] Coates, A.J., et al., 2003. In-orbit results from the SNAP-1 nanosatellite and its future potential. Philos. Trans. R. Soc. London, Ser. A 361 (1802), 199−203.

[4] Nguyen, H., Kohler, J., Stenmark, L., 2002. The merits of cold gas micropropulsion in state-of-the-art space missions. In: 53rd International Astronautical Congress.

[5] Hejmanowski, N., et al., 2015. CubeSat high impulse propulsion system (CHIPS). In: 62nd JANNAF Propulsion Meeting.

[6] Hejmanowski, N., et al., 2016. CubeSat high impulse propulsion syste (CHIPS) design and performance. In: 63rd JANNAF Propulsion Meeting.

[7] Gibbon, D., Ward, J., Kay, N., 2000. The design, development and testing of a propulsion system for the SNAP-1 nanosatellite. In: 14th AIAA/USU Conference on Small Satellites.

[8] Gibbon, D., Underwood, C.I., 2001. Low cost butane propulsion systems for small spacecraft. In: 15th AIAA/USU Conference on Small Satellites.

[9] Hinkley, D.A., 2008. Novel cold gas propulsion system for nanosatellites and picosatellites. In: 22nd AIAA/USU Conference on Small Satellites.

[10] Rankin, D., et al., 2005. The CanX-2 nanosatellite: expanding the science abilities of nanosatellites. Acta Astronaut. 57 (2), 167−174.
[11] Sarda, K., et al., 2008. Canadian advanced nanospace experiment 2 - on-orbit experiences with a 3 kg satellite. In: 22nd AIAA/USU Conference on Small Satellites.
[12] Grönland, T.-A., et al., 2007. Miniaturization of components and systems for space using MEMS-technology. Acta Astronaut. 61 (1), 228−233.
[13] Persson, S., Veldman, S., Bodin, P., 2009. PRISMA—a formation flying project in implementation phase. Acta Astronaut. 65 (9), 1360−1374.
[14] Guo, J., Bouwmeester, J., Gill, E., 2016. In-orbit results of Delfi-n3Xt: lessons learned and move forward. Acta Astronaut. 121, 39−50.
[15] Bonin, G., et al., 2015. CanX-4 and CanX-5 precision formation flight: mission accomplished. In: 29th AIAA/USU Conference on Small Satellites.
[16] Manzoni, G., Brama, Y.L., 2015. Cubesat micropropulsion characterization in low earth orbit. In: 29th AIAA/USU Conference on Small Satellites.
[17] Wu, S., et al., 2014. TW-1: a cubesat constellation for space networking experiments. In: 6th European CubeSat Symposium.
[18] Arestie, S., Lightsey, E.G., Hudson, B., 2012. Development of A Modular, cold gas propulsion system for small satellite applications. Journal of Small Satellites 1 (2), 63−74.
[19] Cardin, J., Day, C., 2020. A standard micro propulsion system for CubeSats. In: CubeSat Developers Workshop.
[20] Perez, L.L., Koch, P., Walker, R., 2018. GOMX-4 − the twin European mission for IOD purposes. In: 32nd AIAA/USU Conference on Small Satellites.
[21] Chapter 8 - Micropropulsion. In: You, Z. (Ed.), 2018. Space Microsystems and Micro/Nano Satellites. Butterworth-Heinemann, pp. 295−339.
[22] Lemmer, K., 2017. Propulsion for CubeSats. Acta Astronaut. 134, 231−243.
[23] Sarda, K., et al., 2006. Canadian advanced nanospace experiment 2: scientific and technological innovation on a three-kilogram satellite. Acta Astronaut. 59 (1), 236−245.
[24] Stevenson, T., Lightsey, G., 2016. Design and characterization of a 3D-printed attitude control thruster for an interplanetary 6U cubesat. In: 30th AIAA/USU Conference on Small Satellites.
[25] Ranjan, R., et al., 2018. Cold gas propulsion microthruster for feed gas utilization in micro satellites. Appl. Energy 220, 921−933.
[26] Cheah, K.H., Chin, J.K., 2014. Fabrication of embedded microstructures via lamination of thick gel-casted ceramic layers. Int. J. Appl. Ceram. Technol. 11 (2), 384−393.
[27] Malik, A.M., et al., 2013. Deep reactive ion etching of silicon moulds for the fabrication of diamond x-ray focusing lenses. J. Micromech. Microeng. 23 (12), 125018.
[28] Chaalane, A., et al., 2015. A MEMS-based solid propellant microthruster array for space and military applications. J. Phys. Conf. 660, 012137.
[29] Louwerse, M.C., et al., 2009. Nozzle fabrication for micropropulsion of a microsatellite. J. Micromech. Microeng. 19 (4), 045008.
[30] Li, H., et al., 2018. Fabrication of ZrB2−SiC−graphite ceramic micro-nozzle by micro-EDM segmented milling. J. Micromech. Microeng. 28 (10), 105022.
[31] Louisos, W.F., Hitt, D.L., 2008. Viscous effects on performance of two-dimensional supersonic linear micronozzles. J. Spacecraft Rockets 45 (4), 706−715.
[32] Ketsdever, A.D., et al., 2005. Experimental and numerical determination of micropropulsion device efficiencies at low Reynolds numbers. AIAA J. 43 (3), 633−641.
[33] Cheah, K.H., Chin, J.K., 2011. Performance improvement on MEMS micropropulsion system through a novel two-depth micronozzle design. Acta Astronaut. 69 (1), 59−70.

[34] Louisos, W., Hitt, D., 2008. Numerical studies of thrust production in 2-D supersonic Bell micronozzles. In: 44th AIAA/ASME/SAE/ASEE Joint Propulsion Conference & Exhibit.
[35] Zilic, A., Hitt, D., Alexeenko, A., 2007. Numerical simulations of supersonic flow in a linear aerospike micro nozzle. In: 37th AIAA Fluid Dynamics Conference and Exhibit.
[36] Louisos, W.F., et al., 2008. Design considerations for supersonic micronozzles. Int. J. Manuf. Res. 3 (1).
[37] Stein, W., Alexeenko, A., 2008. Application of the DSMC method for design of a coaxial microthruster nozzle. In: 44th AIAA/ASME/SAE/ASEE Joint Propulsion Conference & Exhibit.
[38] La Torre, F., et al., 2011. Hybrid simulations of rarefied supersonic gas flows in micronozzles. Comput. Fluid 49 (1), 312−322.
[39] Pearl, J., Louisos, W.F., Hitt, D.L., 2015. Three-dimensional numerical study of linear plug micronozzles. In: 53rd AIAA Aerospace Sciences Meeting.
[40] Ganani, C.S., 2019. Micronozzle Performance A Numerical and Experimental Study. Delft University of Technology.